Analyst

ROYAL SOCIETY OF CHEMISTRY

PAPER

View Article Online
View Journal | View Issue

Cite this: *Analyst*, 2022, **147**, 1986

Preparation of a disposable electrochemiluminescence sensor chip based on an MXene-loaded ruthenium luminescent agent and its application in the detection of carcinoembryonic antigens

Weiwei Luo,[a,b] Zhuoxin Ye,[a] Pinyi Ma, *[a] Qiong Wu*[c] and Daqian Song *[a]

Carcinoembryonic antigen (CEA) is an important cancer marker that plays a significant role in achieving low-cost, rapid and highly sensitive clinical detection. In this work, we developed a disposable electrochemiluminescence (ECL) sensor chip based on a screen-printed electrode (SPE) for detecting CEA *via* ECL technology. An amino-modified Ti_3C_2 MXene was used as a carrier to successfully prepare a highly efficient ECL probe AuNPs-Ru-Arg@NH_2-Ti_3C_2-MXene by loading with AuNPs-Arg through covalent links and modifying with a ruthenium complex. Upon the addition of CEA, the ECL signal decreased significantly with the increase of CEA, due to the formation of immune complexes at the interface of the electrode. The sensing chip was used to detect CEA in an aqueous solution and found to have a detection limit of 1.5 pg mL^{-1}. The chip was used to determine CEA in the serum of healthy humans and cancer patients, and the results were consistent with those obtained using ELISA. The disposable ECL sensor chip has many advantages including convenience, rapid detection, low cost and easy mass production; thus it has great application potential in clinical cancer diagnosis.

Received 14th March 2022,
Accepted 3rd April 2022

DOI: 10.1039/d2an00450j

rsc.li/analyst

1. Introduction

Cancer is a malignant human disease that has the second highest incidence rate after heart disease. Carcinoembryonic antigen (CEA) is a glycoprotein produced by human tumor cells and is one of the common markers for clinical diagnosis and cancer treatment.[1] Many reports have shown that the serum CEA levels in patients with gastric cancer, liver cancer and colorectal cancer are significantly higher than those in healthy individuals.[2–4] When the concentration of CEA in the serum of humans is higher than 20 ng mL^{-1}, it is highly likely that tumors are present in the body.[5] Therefore, a tool that can detect the level of CEA in serum with high selectivity and sensitivity can be of great significance in clinical examination and pathological research. Currently, with the development of analytical techniques, many methods for CEA detection in real samples have been reported. These methods include fluorescence immunoassay,[6] electrochemical analysis,[7] chemiluminescence immunoassay,[8] and surface plasmon resonance.[9] However, convenient and low-cost methods are still required in clinical diagnosis.

The sensitivity and accuracy of the analytical method play significant roles in the early detection of low-abundance and complex samples. Electrochemiluminescence (ECL) is considered as a simple, sensitive and accurate electrochemical reaction analysis tool that has been widely used in immunoassay and DNA probes.[10–14] It has many advantages such as high sensitivity, wide linear ranges, simple operation and low background signals. A Ru complex system plays an important role in ECL application due to its high luminescence efficiency, good water solubility, high stability, reversible single electron transfer reaction and repeatable excitation ability.[15] However, most Ru complex-based ECL systems are used in the solution phase, which can undoubtedly reduce the luminescence efficiency. Therefore, the ECL efficiency of Ru complexes can effectively be improved by introducing functionalized nanomaterials as carriers so that it can be applied in the field of bioanalysis.[16,17]

In recent years, MXenes, two-dimensional nanomaterials containing transition metals, have gained extensive attention from analytical chemists due to their unique structures, as well as their mechanical, electronic, optical and thermal properties.[18–20] The most significant characteristics of MXenes

[a]*College of Chemistry, Jilin Province Research Center for Engineering and Technology of Spectral Analytical Instruments, Jilin University, Qianjin Street 2699, Changchun, 130012, China. E-mail: mapinyi@jlu.edu.cn, songdq@jlu.edu.cn*
[b]*School of Chemistry and Life Science, Anshan Normal University, Ping'an Street 43, Anshan 114005, China*
[c]*Department of Gastrointestinal and Colorectal Surgery, China-Japan Union Hospital of Jilin University, Sendai Street 126, Changchun, 130033, China. E-mail: qiong_wu@jlu.edu.cn*

include high conductivity, good hydrophilicity, chemical stability, high specific surface area, adjustable and abundant surface functional groups, easy synthesis in water, environmental friendliness and nontoxicity.[21–23] However, thus far, there are only a few reports on the use of MXenes as carriers to load Ru complex ECL luminescent groups. Considering its excellent conductivity and large specific surface area, the introduction of an MXene into an ECL probe during construction should greatly and undoubtedly enhance the efficiency of the probe.[24]

Based on the above analysis, we used an amino-modified Ti_3C_2 MXene as a carrier to successfully prepare a highly efficient ECL probe AuNPs-Ru-Arg@NH_2-Ti_3C_2-MXene by loading with AuNPs-Arg through covalent links and modifying with a Ru complex. The unique nanostructure of NH_2-Ti_3C_2-MXene allowed the luminescent reagent carrier to have high carrying capacity. After being covalently modified with L-Arg, the Ru complex had self-enhanced ECL luminescence.[25] The introduction of AuNPs by electrostatic interactions provided a large number of binding sites for biomolecules.[26] A biosensor chip with low price, convenient operation, easy integration and large-scale application could be obtained by modifying the ECL probe onto a screen-printed electrode (SPE).[27,28] A disposable ECL sensor chip for CEA determination was constructed by dripping anti-CEA onto an SPE electrode. After combining with CEA, the number of immune complexes formed at the electrode interface increased, causing an enhancement of the blocking effect on electron transmission;[29] as a result, the ECL signal decreased. Therefore, by changing the concentration of CEA, the ECL intensity gradually changed, and the detection was realized. Finally, we employed the disposable ECL sensor chip to detect serum CEA in healthy individuals and cancer patients, for which satisfactory results were obtained.

2. Experimental section

2.1 Reagents and materials

$[Ru(bpy)_2(mcpbpy)]Cl_2$ was purchased from SunaTech Inc. (Suzhou, China). L-Arginine (L-Arg), 1-ethyl-3-(3-dimethylaminopropyl) carbodiimide hydrochloride (EDC), and sulfo-*N*-hydroxy succinimide (sulfo-NHS) were purchased from Aladdin Reagent Corporation (Shanghai, China). Bovine serum albumin (BSA), immunoglobulin G (IgG), and alpha-fetoprotein (AFP) were from DingGuo Biotechnology Company. The Ti_3AlC_2 MAX phase was from Carbon-Ukraine Ltd. (3-Aminopropyl)triethoxysilane (APTES) and hydrogen tetrachloroaurate hydrate ($HAuCl_4{\cdot}3H_2O$) were from J&K Chemicals. Carcinoembryonic antigen (CEA) and monoclonal anti-CEA were from Fitzgerald Industries. The screen-printed electrode (SPE) was customized from Qingdao Poten Technology Co., Ltd (Qingdao, China). Phosphate-buffered solution (PBS, 0.1 M, pH 7.4) was prepared using Na_2HPO_4 (0.1 M), KH_2PO_4 (0.1 M), and KCl (0.1 M). The rest of the chemicals were analytical reagents of preferable grade and all aqueous solutions were prepared with ultrapure water (≥18 MΩ cm). Human serum samples were from the China–Japan Union Hospital of Jilin University. All experiments were performed in accordance with the Guidelines "Ethical review methods for biomedical research involving people", and approved by the ethics committee at Jilin University.

2.2 Instruments

Cyclic voltammetry (CV) and electrochemical impedance spectroscopy (EIS) experiments were performed using a CHI 760E electrochemical workstation (CH Instruments Ins., China). ECL experiments were performed using a model MPI-A ECL analyzer with a wavelength range of 300–650 nm (Xi'an Remex Analysis Instruments Co., Ltd, China). The surface morphology of NH_2-Ti_3C_2-MXene nanosheets was characterized using a Hitachi SU-8020 scanning electron microscope (SEM, Hitachi Ltd, Japan). NH_2-Ti_3C_2-MXene nanosheets, AuNPs and the AuNPs-Ru-Arg@NH_2-Ti_3C_2-MXene nanocomposite were characterized using a Hitachi H800 transmission electron microscope (TEM, Hitachi Ltd, Japan). The powder X-ray diffraction (XRD) patterns were obtained on an X'pert Pro X-ray diffractometer (PANalytical, Holland) with Cu Kα1 radiation (λ = 1.5406 Å) over a 2θ range of 5–80°. The pH was measured using a pH meter (INESA Scientific, China). Absorbance experiments were performed using a Cary 60 UV-spectrophotometer (Agilent Technologies, USA).

2.3 Synthesis of NH_2-Ti_3C_2-MXene

Ultrathin Ti_3C_2 MXene nanosheets were prepared according to a method reported in the literature.[30] The synthesized Ti_3C_2-Mxene was amino-modified with APTES. 3 mL of ethanol and 12 mL of ultrapure water were added to 30 mg of Ti_3C_2 MXene, and the dispersion was mixed by ultrasonication. After 200 μL of APTES was slowly added, the dispersion was stirred at room temperature for 24 h.[31] After centrifugation, the sample was washed several times with ultrapure water and was subsequently vacuum-dried at 50 °C overnight to obtain a black powder. The purified product was then dispersed in ultrapure water to obtain an NH_2-Ti_3C_2-MXene solution at a concentration of 0.5 mg mL^{-1}. The solution was stored at 4 °C until subsequent use.

2.4 Synthesis of AuNPs-Ru-Arg

$[Ru(bpy)_2(mcpbpy)]Cl_2$ (14.8 mg) was dissolved in 1 mL of ultrapure water, and 8.6 mg of sulfo-NHS and 30.6 mg of EDC were then added to activate carboxyl at 4 °C for 2 h. 7 mg of L-Arg were added, and the mixture was continuously stirred for 4 h to obtain a Ru-Arg complex. The obtained complex solution was dialyzed in a dialysis bag (molecular weight cut off: 100–500) for 4 h, and the final product was diluted with 2 mL of ultrapure water. AuNPs with a size of 50 nm were synthesized by reducing $HAuCl_4$ with citrate. 10 mL of AuNP solution was added to 100 μL of Ru-Arg complex solution, and the mixture was stirred at room temperature for 0.5 h until a black precipitate was formed. After centrifugation and rinsing with water, the AuNPs-Ru-Arg complex was obtained. The complex

was redispersed in 10 mL of ultrapure water and then stored at 4 °C until later use.

2.5 Fabrication of the AuNPs-Ru-Arg@NH_2-Ti_3C_2-MXene nanocomposite

While shaking, 2 mL of NH_2-Ti_3C_2-MXene solution was added dropwise to AuNPs-Ru-Arg solution at the same volume. The mixture was shaken overnight on a shaker. The sample was then centrifuged at 7000 rpm, washed several times with ultrapure water, redispersed in 2 mL ultrapure water, and then stored at 4 °C until subsequent use.

2.6 Preparation of a disposable ECL sensor chip

In this experiment, a PET screen-printed electrode (SPE) integrated with three electrodes including a working electrode (carbon), a counter electrode (carbon), and a reference electrode (Ag/AgCl) was utilized to construct a disposable sensor chip. Firstly, the SPE electrode was pretreated and washed successively with ultrapure water, alcohol, and a mixture of ultrapure water and alcohol at a ratio of 1 : 1. In 0.05 M H_2SO_4 solution, the electrode was subjected to cyclic voltammetry scanning at a voltage range of 0.5 to 1.1 V and a scanning speed of 0.1 V s^{-1} until a stable CV curve was obtained, after which, the electrode was dried for later use.[26] After AuNPs-Ru-Arg@NH_2-Ti_3C_2-MXene suspension (10 μL) was added dropwise and the treated SPE working electrode was dried at room temperature. Then, 10 μL of anti-CEA at a concentration of 100 μg mL^{-1} was added dropwise, and after incubating at 4 °C for 12 h, the modified electrode anti-CEA/AuNPs-Ru-Arg@NH_2-Ti_3C_2-MXene was obtained. To block nonspecific adsorption, BSA (5 μL, 10 mg mL^{-1}) was added to the surface of the electrode, and the electrode was incubated at room temperature for 1 h. After each modification step, the electrode was washed with PBS (0.1 M, pH 7.4). Finally, the obtained ECL sensing chip was stored at 4 °C until subsequent experiments.

2.7 Detection of CEA

Firstly, CEA antigen solutions at different concentrations were prepared with PBS (0.1 M, pH 7.4). CEA at different concentrations or treated sample solution (10 μL each) was added dropwise to the working electrode, and the electrode was incubated at 37 °C for 1 h. Then, the surface of the electrode was rinsed with PBS. SPE was placed in a small beaker containing 10 mL of PBS (0.1 M, pH 7.4), and the ECL detection was performed. The voltage of the photomultiplier tube was set at 800 V. The sample was scanned at 0.2–1.3 V at a scanning speed of 0.1 V s^{-1}.

3. Results and discussion

3.1 Characterization of the materials

First, the obtained Ti_3C_2-MXene nanosheets were analyzed by XRD to identify their crystal structure (Fig. 2a). Several sharp diffraction peaks are located at 6.1°, 18.2°, 30.4°, 36.9°, 43.0°, and 69.6° in the XRD pattern, which is consistent with a previous report.[30] As can be observed in the SEM image (Fig. 1a), after being functionalized with APTES, the surface of the Ti_3C_2-Mxene nanosheets was transparent and smooth. A slight overlap between the sheets could also be observed. This is mainly due to the shear force generated during stirring, which can result in a slight decrease of flatness of the sheets. According to the TEM images, the NH_2-Ti_3C_2-MXene nanosheets had thin, stratified structures (Fig. 2b). Based on the TEM image shown in Fig. 2c, the average diameter of AuNPs was about 50 nm. The Ru complex covalently linked with L-Arg was positively charge and thus was able to combine

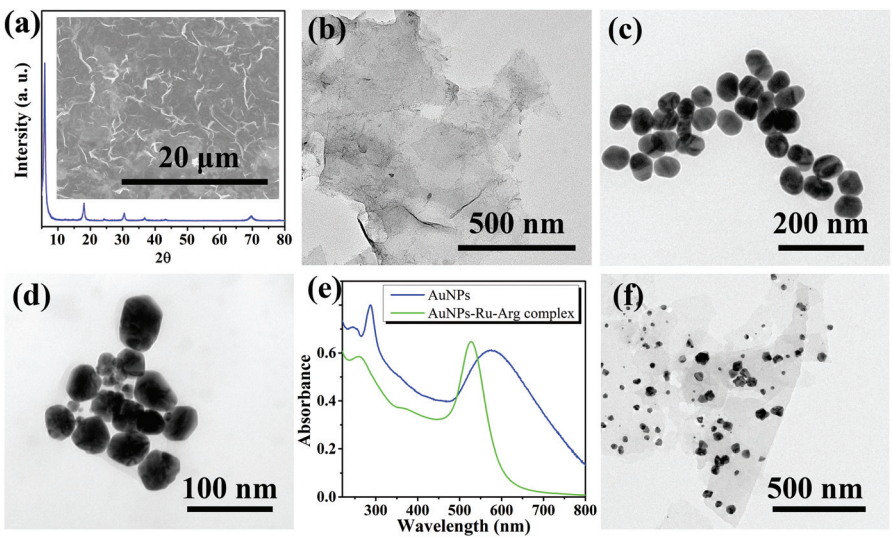

Fig. 1 (a) XRD pattern of Ti_3C_2-MXene nanosheets, and an SEM image of NH_2-Ti_3C_2-MXene nanosheets. (b) TEM image of NH_2-Ti_3C_2-MXene nanosheets. (c) TEM image of AuNPs. (d) TEM image of the AuNPs-Ru-Arg complex. (e) UV-Vis spectra of AuNPs and the AuNPs-Ru-Arg complex. (f) TEM image of the AuNPs-Ru-Arg@NH_2-Ti_3C_2-MXene nanocomposite.

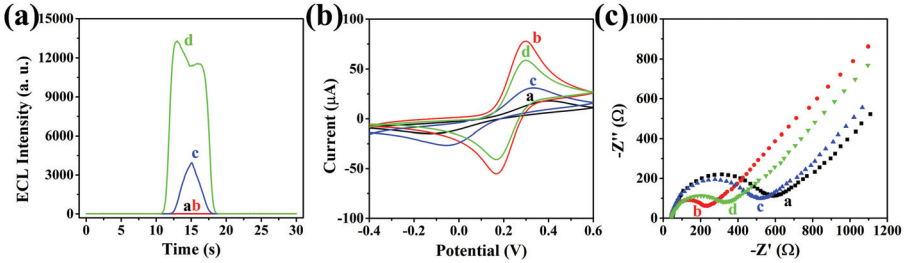

Fig. 2 ECL response in 0.1 M PBS (pH 7.4) (a), CV (b) and EIS (c) of the modified SPE in 0.1 M KCl solution containing 5 mM $[Fe(CN)_6]^{3-/4-}$. a: Bare SPE. b: NH_2-Ti_3C_2-MXene. c: AuNPs-Ru-Arg. d: AuNPs-Ru-Arg@NH_2-Ti_3C_2-MXene.

with negatively charged AuNPs through electrostatic interactions. The TEM image (Fig. 1d) showed that the diameter of the AuNPs-Ru-Arg complex was still 50 nm. The UV-Vis spectrum (Fig. 1e) showed that the absorption peak of AuNPs in the AuNPs-Ru-Arg complex was slightly red-shifted and wider compared with that of uncomplexed AuNPs at 520 nm, and the characteristic absorption peak of the Ru complex appeared at 284 nm.

Amino groups on the surface of NH_2-Ti_3C_2-MXene nanosheets were found connecting to the AuNPs-Ru-Arg complex through Au–N covalent bonds. In addition, the zeta potential results indicated that the NH_2-Ti_3C_2-MXene nanosheets were positively charged, while the AuNPs-Ru-Arg complex was negatively charged. Thus, it is likely that the two tightly bind to one another through electrostatic interactions. The fabricated AuNPs-Ru-Arg@NH_2-Ti_3C_2-MXene nanocomposite was characterized by TEM. As can be seen in Fig. 1f, AuNPs-Ru-Arg was bound to the surface of NH_2-Ti_3C_2-MXene, an indication that the nanocomposite was successfully prepared.

3.2 Performance of the materials

To study the effect of NH_2-Ti_3C_2-MXene as a carrier on the electrochemiluminescence of AuNPs-Ru-Arg, ECL tests were performed on bare SPE electrodes, NH_2-Ti_3C_2-MXene nanosheets, AuNPs-Ru-Arg, and AuNPs-Ru-Arg@NH_2-Ti_3C_2-MXene nanocomposites. According to the results displayed in Fig. 2a, the luminescence intensity of AuNPs-Ru-Arg@NH_2-Ti_3C_2-MXene nanocomposites was about 7 times higher than that of AuNPs-Ru-Arg under the same conditions. This suggests that the introduction of the MXene could greatly improve the luminescence efficiency of Ru complexes.

According to the literature,[32–34] the ECL luminescence mechanism of AuNPs-Ru-Arg@NH_2-Ti_3C_2-MXene nanocomposites may be as follows:

$$[\text{AuNPs-Ru(II)-Arg@NH}_2\text{-Ti}_3\text{C}_2\text{-MXene}] - e^- \rightarrow [\text{AuNPs-Ru(III)-Arg@NH}_2\text{-Ti}_3\text{C}_2\text{-MXene}]$$

$$\text{L-Arg} - e^- \rightarrow \text{L-Arg}^+$$

$$\text{L-Arg}^{\bullet+} \rightarrow \text{L-Arg}^{\bullet} + H^+$$

$$[\text{AuNPs-Ru(III)-Arg@NH}_2\text{-Ti}_3\text{C}_2\text{-MXene}] + \text{L-Arg}^{\bullet} \rightarrow [\text{AuNPs-Ru(II)-Arg@NH}_2\text{-Ti}_3\text{C}_2\text{-MXene}]^* + \text{L-Arg}$$

$$[\text{AuNPs-Ru(II)-Arg@NH}_2\text{-Ti}_3\text{C}_2\text{-MXene}]^* \rightarrow [\text{AuNPs-Ru(II)-Arg@NH}_2\text{-Ti}_3\text{C}_2\text{-MXene}] + h\nu$$

To explain the mechanism by which the MXene promotes the luminescence efficiency of AuNPs-Ru-Arg, we further conducted CV and EIS tests on AuNPs-Ru-Arg@NH_2-Ti_3C_2-MXene nanocomposites using 5 mM $[Fe(CN)_6]^{3-/4-}$ solution containing 0.1 M KCl as the working electrolyte. The results are shown in Fig. 2b. Comparison of the CV curves showed that the MXene-modified SPE electrode had the highest redox peak current, which is likely due to the excellent conductivity and large specific surface area of NH_2-Ti_3C_2-MXene. The redox peak current of the AuNPs-Ru-Arg@NH_2-Ti_3C_2-MXene nanocomposite-modified electrode was slightly lower than that of NH_2-Ti_3C_2-MXene. This observation is likely attributed to the repulsion effect of a large number of negative charge pairs at the electrode surface in $[Fe(CN)_6]^{3-/4-}$, which can hinder the transfer of electrons.[35] Compared with the bare SPE electrode and AuNPs-Ru-Arg-modified electrode, both NH_2-Ti_3C_2-MXene and AuNPs-Ru-Arg@NH_2-Ti_3C_2-MXene had better electron transfer abilities, which is a further indication that an MXene could feasibly be used as a conductive channel to construct an ECL luminescent probe. In addition, the EIS test was mainly used to characterize the conductivity of different materials *via* monitoring the electron transfer resistance R_{et} at the surface of the electrode. Similar to the CV results, Fig. 2c shows that the NH_2-Ti_3C_2-MXene-modified SPE exhibited a very small semicircle, suggesting that it can rapidly transfer electrons. The introduction of negatively charged AuNPs-Ru-Arg caused the electrostatic repulsion of AuNPs-Ru-Arg@NH_2-Ti_3C_2-MXeneto $[Fe(CN)_6]^{3-/4-}$ to increase, in turn causing the R_{et} to increase. However, the impedance of this composite was still lower than that of the bare SPE electrode and AuNPs-Ru-Arg-modified electrode. These EIS results indicate that the introduction of the MXene can effectively increase the electron transfer efficiency due to the special nanostructure and large specific surface area of the MXene.[36] Based on the above results, the prepared ECL luminescent material has excellent luminescence properties, and the MXene appears to play a key role in

the properties. On the one hand, as an ideal electronic conductor, the MXene can greatly improve the electron transfer rate on the electrode surface. On the other hand, the large specific surface area of the MXene not only is conducive to mass transfer, but also can be used as an efficient nanocarrier for loading of a large quantity of the luminescent reagent AuNPs-Ru-Arg, thereby allowing an enhancement of the ECL signal.

3.3 Construction of an ECL sensing system

Based on the above results, we further constructed a disposable ECL sensor chip from the AuNPs-Ru-Arg@NH_2-Ti_3C_2-MXene nanocomposite, and then used it in CEA detection. The detection principle of the ECL sensor chip is shown in Fig. 3. Ru complexes have excellent electrochemiluminescence properties, and L-Arg can be used as a co-reactant. The covalent link between Ru and L-Arg can lead to the self-enhancement of the ECL signal. The AuNPs-Ru-Arg complex is formed through the electrostatic interaction between AuNPs and Ru-Arg, and the introduction of AuNPs can provide a large number of binding sites for biomolecules. The large specific surface area and superior conductivity of the MXene material allow an increase of the electron transfer efficiency. The amino-modified MXene allows higher loading of the AuNPs-Ru-Arg complex; thus, the electrode can exhibit stronger ECL signals. A disposable ECL sensor chip was constructed by successively dripping the AuNPs-Ru-Arg@NH_2-Ti_3C_2-MXene nanocomposite, anti-CEA and BSA onto the pretreated working SPE electrode. When the electrode surface is modified with an antibody and then combined with CEA, the electron transfer and the diffusion of the electrolyte on the electrode surface can be hindered due to the insulation of protein molecules and the steric hindrance of the antigen–antibody conjugate. As a result, the ECL signal is decreased. This shows that the intensity of ECL can be changed by gradually changing the concentration of CEA, allowing the detection to be realized.

The sensing process of the ECL sensing system was characterized by CV, ESI and ECL. As can be seen in the CV curve (Fig. 4a), after anti-CEA, BSA, and CEA were sequentially assembled on the surface of the AuNPs-Ru-Arg@NH_2-Ti_3C_2-MXene-modified electrode, the redox peak current was gradually decreased, indicating that the sensor was successfully constructed. The EIS results also showed the same trend (Fig. 4b). After anti-CEA was incubated on the electrode surface, the electron transfer on the electrode surface was hindered; therefore, the R_{et} of the electrode was significantly increased. Subsequently, BSA, which was used to block non-specific binding, became non-conductive, causing the R_{et} to further increase. Finally, the antigen–antibody complex was formed after CEA was modified on the electrode surface, which further hindered the electron transfer, causing the R_{et} to reach its maximum value. Each of the above steps is an indicator that the electrochemical sensor was successfully constructed. We

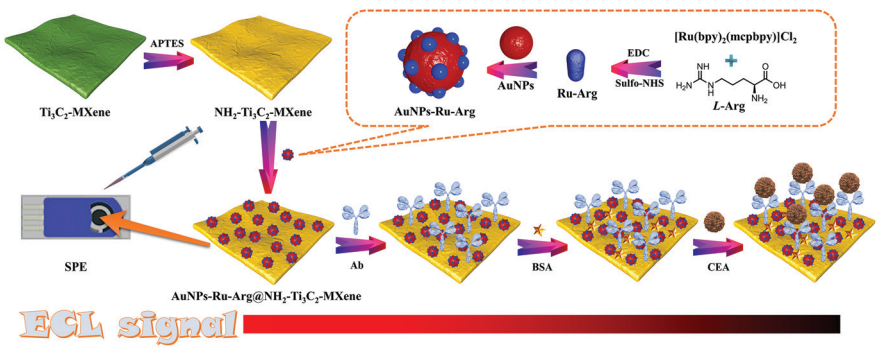

Fig. 3 Schematic representation showing the detection principle of the prepared ECL biosensor.

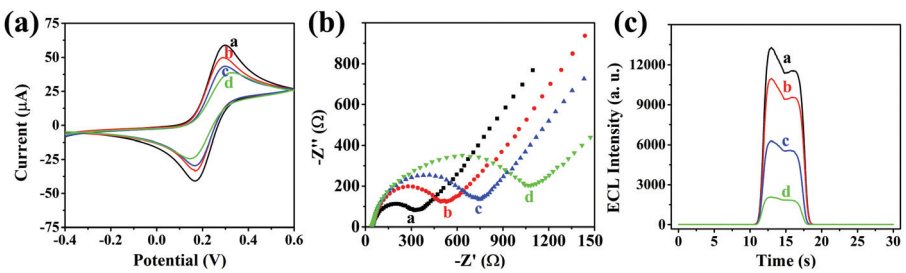

Fig. 4 Characterization by (a) CV and (b) EIS in 0.1 M KCl solution containing 5 mM $[Fe(CN)_6]^{3-/4-}$ and (c) ECL response in 0.1 M PBS (pH 9.4) of the modified SPE. a: AuNPs-Ru-Arg@NH_2-Ti_3C_2-MXene. b: AuNPs-Ru-Arg@NH_2-Ti_3C_2-MXene/anti-CEA. c: AuNPs-Ru-Arg@NH_2-Ti_3C_2-MXene/anti-CEA/BSA. d: AuNPs-Ru-Arg@NH_2-Ti_3C_2-MXene/anti-CEA/BSA/CEA. Anti-CEA: 10 μL at 100 μg mL^{-1}. BSA: 5 μL at 10 mg mL^{-1}. CEA: 10 μL at 10 ng mL^{-1}.

further characterized the performance of the sensor through its ECL signal. As shown in Fig. 4c, after anti-CEA and BSA were modified on the electrode surface, the ECL intensity decreased significantly. After being further modified with CEA, the ECL intensity further decreased, which is an indication that the ECL sensing system could be used for CEA detection. In addition, compared with CV and EIS, the ECL system had higher sensitivity, suggesting that it is a better detection system.

3.4 Performance of the ECL sensor chip

Firstly, we investigated the influence of time for the incubation of CEA and AuNPs-Ru-Arg@NH_2-Ti_3C_2-MXene/anti-CEA/BSA on the SPE sensor chip on the ECL signal. As shown in Fig. 5a, the ECL signal gradually decreased with the increase of incubation time, and the luminescence intensity was rather stable after 1 h, which indicates that the formation of the antigen–antibody complex was nearly complete within 1 h. Therefore, 1 h was selected as the optimal time in CEA detection experiments.

Under the optimum conditions, CEA solutions at different concentrations were added onto the surface of the working electrode, and after incubating for 1 h, the ECL signal was measured. As shown in Fig. 5b, the ECL signal intensity gradually decreased with the increase of CEA concentration, reaching a plateau after the CEA concentration reached 200 ng mL^{-1}. When the concentration of CEA was between 0.01 and 150 ng mL^{-1}, the ECL signal and log CEA concentration had a linear relationship (Fig. 5c) with a linear equation $I = -1179.65 \times \lg[\text{CEA}] + 3374.29$ (Fig. 5(b)), $r = 0.9991$; and the detection limit (3σ) was 1.5 pg mL^{-1}. Table 1 shows the results from different CEA detection methods. The comparison showed that our sensor chip exhibited better analytical performance, a wider detection range and a lower detection limit. Compared to other ECL immunosensors (Table 2), we used disposable SPE electrodes to avoid tedious pretreatment steps, which make our sensor simple and more repeatable than GCE electrodes, and can be used for rapid detection.

Stability and reproducibility are key evaluators that can be used to evaluate the practical application of an ECL sensing

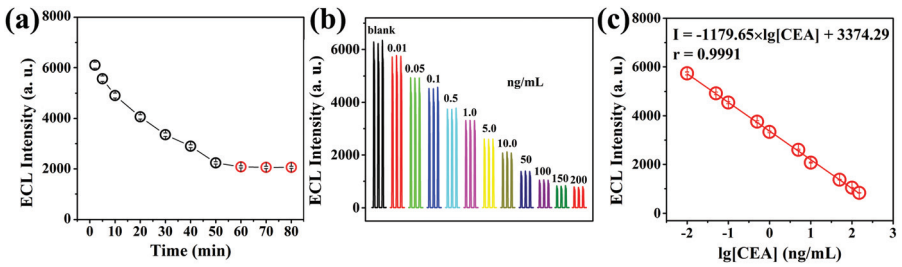

Fig. 5 (a) Variation of the ECL intensity of 10 ng mL^{-1} CEA with cleavage time detected with the ECL biosensor. (b) Response of the ECL biosensor to the presence of CEA at different concentrations: 0, 0.01, 0.05, 0.1, 0.5, 1.0, 5.0, 10.0, 50.0, 100.0, 150.0, and 200.0 ng mL^{-1}. (c) Calibration curve used for determining the CEA concentration.

Table 1 Comparison of different methods used for the detection of CEA

Methods	Strategies	Detection range (ng mL^{-1})	LOD (pg mL^{-1})	Ref.
Differential pulse voltammetry	G-quadruplex DNAzyme	2–45	240	37
Surface plasmon resonance	Dual signal amplification	1–1000	100	38
Pressure-based immunoassays	Triple-step signal amplification	0.1–90	81	39
Fluorescence resonance energy transfer	Sandwich-format immunoassay	1.2–490	46	40
Enzyme-linked immunochromatographic sensor	Smartphone-based system	0.031–1.95	16	41
Electrochemical impedance spectroscopy	Aptamer	0.01–10	8.88	42
ECL	Self-enhanced ECL luminescence	0.01–150	1.5	This work

Table 2 Comparison of different ECL immunosensors

ECL immunosensors	Detection range (ng mL^{-1})	LOD (pg mL^{-1})	Ref.
GC-Au-g-C_3N_4 NHs/Ab/BSA/CEA	0.02–80	6.8	43
GCE-G-CdTe/Ab1/CEA/$ZnFe_2O_4$@Au-Ab2	0.01–50	4	44
GCE-AuNP@NPCGO/Ab1/CEA/RuSiNP-Ab2	0.01–80	3	45
GCE-luminol/r-Co_3O_4 NRs/Ab/CEA	0.005–500	2.9	46
GCE-AgNPs/Ab1/CEA/AuNPs/CODs-PEI-GO	0.005–500	1.67	47
SPE-AuNPs-Ru-Arg@NH_2-Ti_3C_2-MXene/Ab/BSA/CEA	0.01–150	1.5	This work

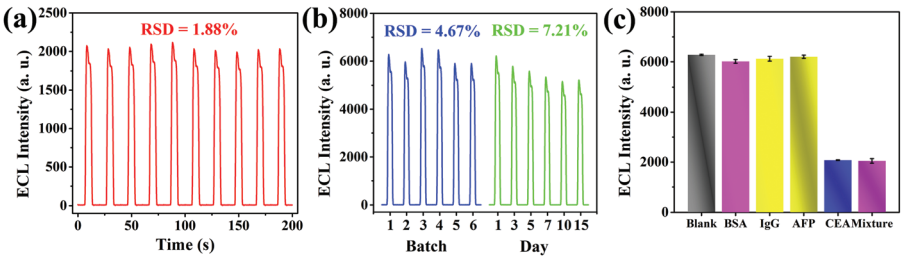

Fig. 6 Stability of the ECL signal after being subjected to continuous scanning for 10 cycles: (a) 10 μL of 10 ng mL^{-1} CEA and (b) 6 batches of electrode, and electrode stored for 15 days. (c) Selectivity of the ECL biosensor towards 10 ng mL^{-1} CEA in the presence of 10 ng mL^{-1} each of interfering substances.

system. CEA at a concentration of 10 ng mL^{-1} was used in this experiment. After 10 cycles of continuous cyclic potential scanning, the ECL signal was not obviously changed, and the RSD was less than 3%. This suggests that the material on the surface of the sensor chip has high stability. The RSD calculated based on SPE electrodes modified with the same material but in different batches was less than 8%, indicating that the sensor chip has high reproducibility. A batch of modified electrodes was stored in a dryer away from light, and the chip was tested daily. The signal of the sensor chip was changed with an RSD of less than 15% after 15 days, an indication that the chip has good reproducibility.

To evaluate the selectivity of the sensing system, we employed several commonly used proteins, such as AFP, BSA and IgG, as interfering substances. At a concentration of 10 ng mL^{-1}, the proteins caused little changes in the ECL signal intensity compared to the blank control. In contrast, the presence of CEA caused the ECL signal intensity to decrease significantly, indicating that the developed sensor chip has high selectivity towards CEA (Fig. 6).

In addition, the SPE electrode utilized in this study is disposable with a low cost of less than $1, does not require pretreatment and is conveniently accessible, and combined with its excellent performance in CEA detection, it may have great commercialization potential.

3.5 Detection of CEA in human serum samples

To assess the practical application of the developed ECL sensor chip, the sensor was used to detect CEA in human serum. The concentrations of CEA in the serum of healthy humans range from 0 to 5.0 ng mL^{-1}, and those in the serum of patients with liver cancer, gastric cancer and colorectal cancer are significantly higher.[48] The clinical monitoring of the CEA concentration can be beneficial for the early diagnosis of cancer, the grading of cancer and the correlation analysis of prognosis.[49] We employed our ECL sensor chip to detect CEA in serum samples of healthy humans, serum samples of healthy humans spiked with CEA (Table 3), and serum samples from 1 patient with gastric cancer, 1 patient with liver cancer and 1 patient with colon cancer, and the results were compared with those obtained from ELISA (Table 4). The comparison showed that the relative deviation between our method and ELISA was less than 8.8% and the recovery rates were between 92.4% and 103%. This shows that our method may have great application potential in clinical cancer diagnosis.

Table 3 Detection of CEA in human serum samples using the ECL sensor chip (n = 3)

Content of CEA (ng mL^{-1})	Spiked (ng mL^{-1})	Detected (ng mL^{-1})	Recovery	RSD
None	0.1	0.103	103%	2.8%
None	1.0	0.96	96%	5.2%
None	10.0	9.37	93.7%	3.7%
None	50.0	46.2	92.4%	6.3%

Table 4 Analysis of serum samples from cancer patients (n = 3)

Samples	Tumor types	Measured (ng mL^{-1})	ELISA	Relative error
1	Gastric cancer	29.6	31.9	7.2%
2	Liver cancer	45.8	49.8	8.0%
3	Colon cancer	125	137	8.8%

4. Conclusions

In summary, we developed a novel type of disposable ECL sensor chip for CEA detection. As a result of insulation by protein molecules and steric hindrance caused by antigen–antibody bioconjugates, the ECL signal of the AuNPs-Ru-Arg@NH_2-Ti_3C_2-MXene nanocomposite-modified SPE electrode was inhibited, making the detection of CEA possible. Furthermore, NH_2-Ti_3C_2-MXene, which has a larger specific surface area and excellent electrical conductivity, was used as a carrier. After being loaded with AuNPs-Ru-Arg, the luminescence intensity was increased by 7 fold. This is the first time an MXene-loaded Ru luminescent material was used to detect CEA through an ECL sensing system, which not only had high sensitivity, but also high stability. The developed sensor chip was employed to detect CEA in human serum, and the operation was rapid and convenient. With its low cost, the chip may have broad applications in cancer diagnosis and prognosis.

Author contributions

Weiwei Luo: investigation, methodology, validation, writing – original draft. Zhuoxin Ye: formal analysis, visualization, writing – review and editing. Pinyi Ma: conceptualization, supervision, funding acquisition, writing – review and editing. Qiong Wu: conceptualization, methodology, validation, writing – review and editing. Daqian Song: supervision, funding acquisition, writing – review and editing.

Conflicts of interest

There are no conflicts to declare.

Acknowledgements

This work was supported by the National Natural Science Foundation of China (Grant No. 22074052 and 22004046).

References

1 M. Grunnet and J. B. Sorensen, *Lung Cancer*, 2012, **76**, 138–143.
2 N. Beauchemin and A. Arabzadeh, *Cancer Metastasis Rev.*, 2013, **32**, 643–671.
3 C. Hall, L. Clarke, A. Pal, P. Buchwald, T. Eglinton, C. Wakeman and F. Frizelle, *Ann. Coloproctol.*, 2019, **35**, 294–305.
4 S. Faias, M. Cravo, P. Chaves and L. Pereira, *Gastrointest. Endosc.*, 2021, **94**, 235–247.
5 X. Gao, Y. Zhang, H. Chen, Z. Chen and X. Lin, *Anal. Biochem.*, 2011, **414**, 70–76.
6 H. Li, L. Shi, D. E. Sun, P. Li and Z. Liu, *Biosens. Bioelectron.*, 2016, **86**, 791–798.
7 Z. Liu and Z. Ma, *Biosens. Bioelectron.*, 2013, **46**, 1–7.
8 S. Pal and S. Bhand, *Microchim. Acta*, 2015, **182**, 1643–1651.
9 T. Springer, M. L. Ermini, B. Spackova, J. Jablonku and J. Homola, *Anal. Chem.*, 2014, **86**, 10350–10356.
10 Y. Cao, C. Ma and J.-J. Zhu, *J. Anal. Test.*, 2021, **5**, 95–111.
11 F. Du, Y. Chen, C. Meng, B. Lou, W. Zhang and G. Xu, *Curr. Opin. Electrochem.*, 2021, **28**, 100725.
12 H. Filik and A. A. Avan, *Curr. Med. Chem.*, 2021, **28**, 3490–3513.
13 H. Nasrollahpour, B. Khalilzadeh, A. Naseri, M. Sillanpaa and C. H. Chia, *Anal. Chem.*, 2022, **94**, 349–365.
14 S. Zhang and Y. Liu, *Front. Chem.*, 2021, **8**, 626243.
15 Z. Liu, W. Qi and G. Xu, *Chem. Soc. Rev.*, 2015, **44**, 3117–3142.
16 J. Zhou, Y. Li, W. Wang, X. Tan, Z. Lu and H. Han, *Biosens. Bioelectron.*, 2020, **164**, 112332.
17 L. Li, Y. Chen and J.-J. Zhu, *Anal. Chem.*, 2017, **89**, 358–371.
18 J. A. Kumar, P. Prakash, T. Krithiga, D. J. Amarnath, J. Premkumar, N. Rajamohan, Y. Vasseghian, P. Saravanan and M. Rajasimman, *Chemosphere*, 2022, **286**, 131607.
19 P. Saravanan, S. Rajeswari, J. A. Kumar, M. Rajasimman and N. Rajamohan, *Chemosphere*, 2022, **286**, 131873.
20 A. C. Ezika, E. R. Sadiku, C. I. Idumah, S. S. Ray and Y. Hamam, *J. Energy Storage*, 2022, **45**, 103686.
21 X. Zhan, C. Si, J. Zhou and Z. Sun, *Nanoscale Horiz.*, 2020, **5**, 235–258.
22 J.-C. Lei, X. Zhang and Z. Zhou, *Front. Phys.*, 2015, **10**, 276–286.
23 A. Sinha, Dhanjai, H. Zhao, Y. Huang, X. Lu, J. Chen and R. Jain, *TrAC, Trends Anal. Chem.*, 2018, **105**, 424–435.
24 X. Wu, P. Ma, Y. Sun, F. Du, D. Song and G. Xu, *Electroanalysis*, 2021, **33**, 1827–1851.
25 Y. Yang, G.-B. Hu, W.-B. Liang, L.-Y. Yao, W. Huang, R. Yuan and D.-R. Xiao, *Nanoscale*, 2019, **11**, 10056–10063.
26 W. Luo, H. Chu, X. Wu, P. Ma, Q. Wu and D. Song, *Talanta*, 2022, **239**, 123083.
27 Z. Taleat, A. Khoshroo and M. Mazloum-Ardakani, *Microchim. Acta*, 2014, **181**, 865–891.
28 K. Fu, R. Zhang, J. He, H. Bai and G. Zhang, *Biosens. Bioelectron.*, 2019, **143**, 111636.
29 L. Li, C. Ma, Q. Kong, W. Li, Y. Zhang, S. Ge, M. Yan and J. Yu, *J. Mater. Chem. B*, 2014, **2**, 6669–6674.
30 Q. Wu, N. Li, Y. Wang, Y. Xu, J. Wu, G. Jia, F. Ji, X. Fang, F. Chen and X. Cui, *Anal. Chem.*, 2020, **92**, 3354–3360.
31 S. Kumar, Y. Lei, N. H. Alshareef, M. A. Quevedo-Lopez and K. N. Salama, *Biosens. Bioelectron.*, 2018, **121**, 243–249.
32 M. Zhao, N. Liao, Y. Zhuo, Y.-Q. Chai, J.-P. Wang and R. Yuan, *Anal. Chem.*, 2015, **87**, 7602–7609.
33 L. Zhang, Y. He, H. Wang, Y. Yuan, R. Yuan and Y. Chai, *Biosens. Bioelectron.*, 2015, **74**, 924–930.
34 Y. Zhuo, N. Liao, Y.-Q. Chai, G.-F. Gui, M. Zhao, J. Han, Y. Xiang and R. Yuan, *Anal. Chem.*, 2014, **86**, 1053–1060.
35 X. Zhu, Q. Zhai, W. Gu, J. Li and E. Wang, *Anal. Chem.*, 2017, **89**, 12108–12114.
36 X. Zhang, L. Wang, W. Liu, C. Li, K. Wang and Y. Ma, *ACS Omega*, 2020, **5**, 75–82.
37 X.-J. Zhai, Q.-L. Wang, H.-F. Cui, X. Song, Q.-Y. Lv and Y. Guo, *Biosens. Bioelectron.*, 2021, **194**, 113618.
38 H. Wang, X. Wang, J. Wang, W. Fu and C. Yao, *Sci. Rep.*, 2016, **6**, 33140.
39 L. Huang, Y. Zeng, X. Liu and D. Tang, *ACS Appl. Mater. Interfaces*, 2021, **13**, 46440–46450.
40 Z. Chen, P. Li, Z. Zhang, X. Zhai, J. Liang, Q. Chen, K. Li, G. Lin, T. Liu and Y. Wu, *Anal. Chem.*, 2019, **91**, 5777–5785.
41 Z. Wu, J. Lu, Q. Fu, L. Sheng, B. Liu, C. Wang, C. Li and T. Li, *Sens. Actuators, B*, 2021, **329**, 129163.
42 C. Guo, F. Su, Y. Song, B. Hu, M. Wang, L. He, D. Peng and Z. Zhang, *ACS Appl. Mater. Interfaces*, 2017, **9**, 41188–41199.
43 L. Chen, X. Zeng, P. Si, Y. Chen, Y. Chi, D. H. Kim and G. Chen, *Anal. Chem.*, 2014, **86**, 4188–4195.
44 L. Shen, C. Chu, C. Ma, H. Yang, S. Ge, J. Yu, M. Yan and X. Song, *Sens. Actuators, B*, 2014, **201**, 196–203.
45 X. Huang, X. Deng, W. Qi and D. Wu, *New J. Chem.*, 2018, **42**, 13558–13564.

46 Y. Tang, B. Zhang, Y. Wang, F. Zhao and B. Zeng, *ACS Appl. Nano Mater.*, 2021, **4**, 7264–7271.
47 N.-L. Li, L.-P. Jia, R.-N. Ma, W.-L. Jia, Y.-Y. Lu, S.-S. Shi and H.-S. Wang, *Biosens. Bioelectron.*, 2017, **89**, 453–460.
48 X.-P. Liu, J.-S. Chen, C.-J. Mao and B.-K. Jin, *Analyst*, 2021, **146**, 146–155.
49 W. Xiang, Q. Lv, H. Shi, B. Xie and L. Gao, *Talanta*, 2020, **214**, 120716.